**Structural Monitoring and Maintenance**, *Vol. 2, No. 1 (2015) 77-93*
DOI: http://dx.doi.org/10.12989/smm.2015.2.1.077 

# Refinement of damage identification capability of neural network techniques in application to a suspension bridge

J.Y. Wang[1a] and Y.Q. Ni[*2]

[1]*Department of Design Management, Hangzhou Construction Committee, Hangzhou, China*
[2]*Department of Civil and Environmental Engineering, The Hong Kong Polytechnic University, Hung Hom, Kowloon, Hong Kong*

*(Received January 23, 2015, Revised March 5, 2015, Accepted March 7, 2015)*

**Abstract.** The idea of using measured dynamic characteristics for damage detection is attractive because it allows for a global evaluation of the structural health and condition. However, vibration-based damage detection for complex structures such as long-span cable-supported bridges still remains a challenge. As a suspension or cable-stayed bridge involves in general thousands of structural components, the conventional damage detection methods based on model updating and/or parameter identification might result in ill-conditioning and non-uniqueness in the solution of inverse problems. Alternatively, methods that utilize, to the utmost extent, information from forward problems and avoid direct solution to inverse problems would be more suitable for vibration-based damage detection of long-span cable-supported bridges. The auto-associative neural network (ANN) technique and the probabilistic neural network (PNN) technique, that both eschew inverse problems, have been proposed for identifying and locating damage in suspension and cable-stayed bridges. Without the help of a structural model, ANNs with appropriate configuration can be trained using only the measured modal frequencies from healthy structure under varying environmental conditions, and a new set of modal frequency data acquired from an unknown state of the structure is then fed into the trained ANNs for damage presence identification. With the help of a structural model, PNNs can be configured using the relative changes of modal frequencies before and after damage by assuming damage at different locations, and then the measured modal frequencies from the structure can be presented to locate the damage. However, such formulated ANNs and PNNs may still be incompetent to identify damage occurring at the deck members of a cable-supported bridge because of very low modal sensitivity to the damage. The present study endeavors to enhance the damage identification capability of ANNs and PNNs when being applied for identification of damage incurred at deck members. Effort is first made to construct combined modal parameters which are synthesized from measured modal frequencies and modal shape components to train ANNs for damage alarming. With the purpose of improving identification accuracy, effort is then made to configure PNNs for damage localization by adapting the smoothing parameter in the Bayesian classifier to different values for different pattern classes. The performance of the ANNs with their input being modal frequencies and the combined modal parameters respectively and the PNNs with constant and adaptive smoothing parameters respectively is evaluated through simulation studies of identifying damage inflicted on different deck members of the double-deck suspension Tsing Ma Bridge.

**Keywords:** structural health monitoring; vibration-based damage identification; auto-associative neural network; probabilistic neural network; suspension bridge

*Corresponding author, Professor, E-mail: ceyqni@polyu.edu.hk
[a] Ph.D.


http://www.techno-press.org/?journal=smm&subpage=7 ISSN: 2288-6605 (Print), 2288-6613 (Online)

## 1. Introduction

All load-carrying structures, including bridges, continuously accumulate damage during their service life. Structural damage is usually caused by degradation and deterioration of structural components and/or connections. Undetected damage might cause catastrophic structural failure. From the viewpoint of serviceability and safety of structures, it is essential to detect the structural damage before failure occurs. Knowledge of damage is also the basis for making decision as to whether retrofitting, partial replacement or demolition is necessary after severe hazards or long-term usage. Visual inspection is the most common method for structural condition assessment and damage detection. However, this method is unreliable for complex structures because certain critical damage may occur in inaccessible areas or may be concealed by paint or skin. The traditional non-destructive testing methods, such as radiographic, X-ray, acoustic emission, and ultrasonic techniques, can only provide deterioration state of local areas.

Over the past two decades there has been great interest in the development of structural health monitoring methodologies using vibration measurements. The idea of using measured dynamic characteristics for damage detection is attractive because it allows for a global evaluation of the structural health and condition even when the damage location is inaccessible. Despite much recent research and some successful applications of SHM technology in recent years (Aktan *et al*. 2001, DeWolf *et al.* 2002, Wong 2004, Ko and Ni 2005, Brownjohn 2007, Catbas 2009, Fujino *et al*. 2009, Glisic *et al*. 2009, Ni *et al.* 2009, Ou and Li 2009, Wang and Yim 2010, Ni *et al.* 2011, Yun *et al.* 2011, Zhou *et al.* 2013, Kim *et al.* 2014, Li *et al.* 2014, Minardo *et al.* 2014), vibration-based damage detection of complex structures (such as long-span cable-supported bridges) using SHM data remains a challenge. The difficulties encountered in the damage assessment of complex civil engineering structures using vibration measurements are primarily due to uncertainty of ambient conditions, insensitivity of global modal properties to local damage, measurement noise, modelling error, and incompleteness of measured modal data.

As a suspension or cable-stayed bridge involves in general thousands of structural components, the conventional damage detection methods based on model updating and parameter identification are usually infeasible for application to this kind of structures because of ill-conditioning and non-uniqueness in the solution of inverse problems. Alternatively, methods that capitalize on, to the utmost extent, information from forward problems and avoid direct solution to inverse problems would be more persuasive for application to large-scale cable-supported bridges for vibration-based damage detection (Ko *et al*. 2002, Yan *et al.* 2004, Ni *et al.* 2008, Oh *et al.* 2009, Zhou *et al.* 2011b). The auto-associative neural network (ANN) technique and the probabilistic neural network (PNN) technique, that both eschew inverse problems, have been proposed for identifying and locating damage in suspension and cable-stayed bridges (Zhou *et al.* 2011a, Zhou *et al.* 2014, Ni *et al.* 2015). In their studies, a series of ‘noisy’ modal frequencies obtained from the healthy structure were used as both input and output to train ANNs configured with ‘bottleneck’ hidden layer(s), and a new series of modal frequencies obtained later from the same structure (damaged or undamaged) were presented to the trained ANNs to identify whether damage had occurred. With the help of a structural model, PNNs were configured in terms of kernel density estimators by setting their weight vectors as the relative changes of modal frequencies when assuming damage at different locations (regions) of the structure; the measured change of modal frequencies was fed into the configured PNNs to locate damage. In application to detecting damage assumed in a suspension bridge and a cable-stayed bridge (Zhou *et al.* 2014, Ni *et al.* 2015), it was found that the afore-formulated ANNs and PNNs were still difficult to identify

damage inflicted on the deck members. The present study endeavors to refine the damage identification capability of ANNs and PNNs by constructing combined modal parameters as both input and output to ANNs and adapting the smoothing parameter in the PNN paradigm to different values for different pattern classes. The Tsing Ma Bridge (TMB) is hereinafter adopted as a 'testbed' for the simulation studies of damage identification in recognizing the fact that this double-deck suspension bridge has very low modal sensitivity to damage at deck members.

## 2. Tsing Ma Bridge and its finite element model

### *2.1 Tsing Ma Bridge (TMB)*

The Tsing Ma Bridge (TMB) is one of the major bridges that constitute traffic artery in Hong Kong. As illustrated in Figs. 1 and 2, the TMB (Beard 1995, Beard and Young 1995) is a double-deck suspension bridge with a main span of 1,377m and an overall length of 2,160 m. It carries six lanes of traffic on its upper deck and two railway tracks and two emergency traffic lanes on its sheltered lower deck. The central span deck and the Ma Wan side span deck are suspended at 18 m intervals by hangers to the main cables in 1.1 m diameter. The Tsing Yi side span deck is instead supported from the ground by three concrete piers spaced at 72 m centers. The two 206 m high towers are reinforced concrete structure, each consisting of two legs connected by four reinforced concrete crossbeams. The steel bridge deck is a continuous structure between anchorages through welding connections of 96 deck units, each generally 18 m long, 41 m wide and 7.5 m high. Structurally the deck section is hybrid arrangement combining both longitudinal trusses and vierendeel cross-frames. Covered with orthotropic deck plates, two 7.2 m deep longitudinal trusses, spaced at 26 m centers, support the carriageways to provide bending stiffness. Vierendeel cross-frames, 4.5 m apart, are supported on longitudinal diagonally braced trusses to carry the railways and longitudinal central vents are provided in the upper and lower deck to enhance stability. Plane diagonal bracing spans the upper and lower vents and acts with the orthotropic plates to provide lateral stiffness. Non-structural, 1.5 mm thick, stainless steel sheeting forms the edge fairing surfaces. The bridge was designed to serve 120 years and to satisfy stringent criteria resulting from Hong Kong's typhoon wind climate.

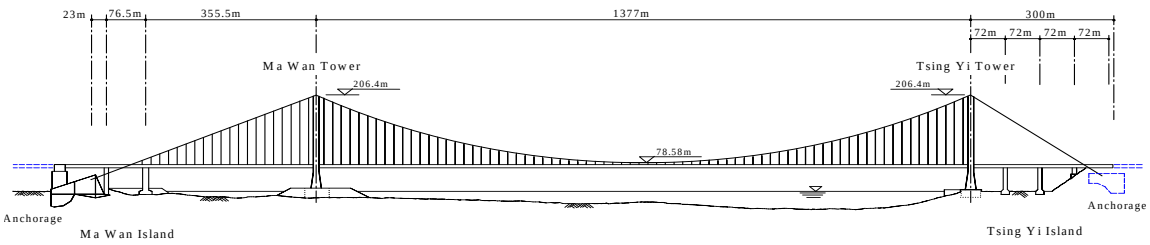


Fig. 1 Tsing Ma Bridge (TMB)

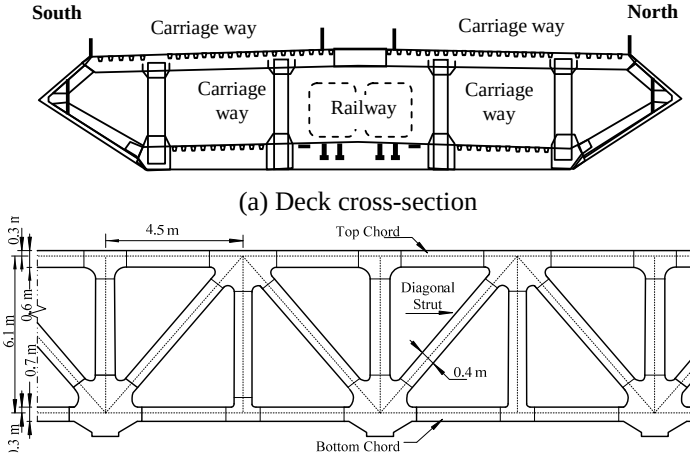


(a) Deck cross-section

(b) Longitudinal trusses

Fig. 2 Double-deck configuration of Tsing Ma Bridge (TMB)

### *2.2 Finite element model*

As shown in Fig. 3, a precise 3D finite element model (FEM) of the TMB, consisting of 17,677 elements and 7,375 nodes, has been developed using the commercial ABAQUS software for damage identification simulation studies. To enable the simulation of damage at deck members, the spatial configuration of the original structure remains in the FEM, and the mass and stiffness contribution of individual structural members is independently described in the FEM such that the sensitivity of global and local modal properties to any structural member can be evaluated accurately. Thus, damage to any structural member can be directly and precisely simulated.

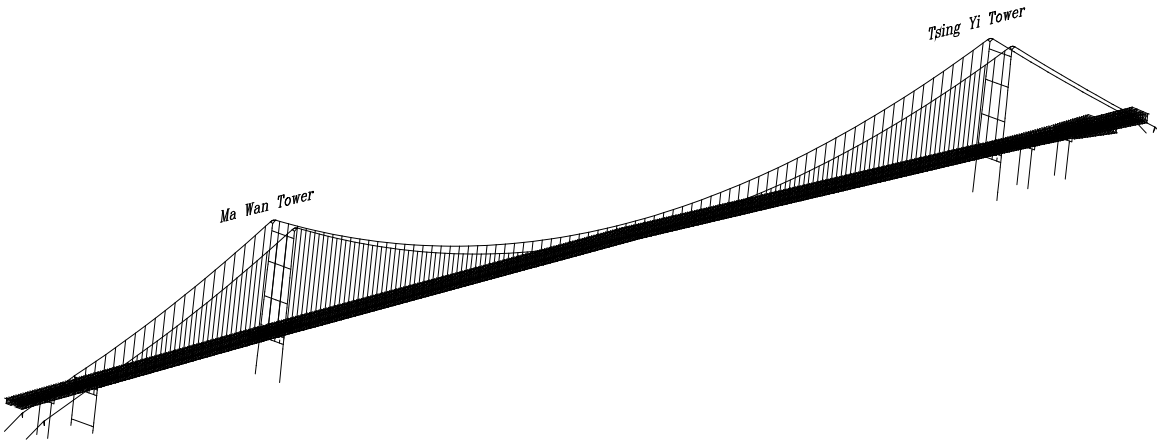


Fig. 3 Finite element model of TMB

With the formulated FEM, modal analysis of the TMB has been conducted. The evaluated modal properties are summarized as follows: (a) the vibration modes are closely spaced, and the predicted modal frequencies of the first 67 modes are less than 1.0 Hz; (b) the fundamental modal frequency of the bridge is as low as 0.069 Hz which corresponds to the first lateral bending mode with the mode shape being a symmetric half-wave in the main span; (c) the first vertical bending mode, with its frequency being 0.115 Hz, is an antisymmetric integral wave in the main span; and (d) the vibration modes of the bridge include global and local modes. Most global modes are three-dimensional and have coupled components in the three directions, especially the lateral bending and torsional modes. The vibration modes of the TMB can be classified into the following seven categories: (i) global vertical bending modes, (ii) global lateral bending and torsion modes, (iii) central span cable local sway modes, (iv) Ma Wan side span cable local sway modes, (v) Tsing Yi side span free cable local modes (in-plane and out-of-plane), (vi) Ma Wan side span deck dominated modes, and (vii) tower dominated modes (sway, bending and torsion).

## 3. Damage alarming by ANNs with different design of input vector

### *3.1 Formulation*

ANNs by using modal frequencies as input vector have been proposed by the authors for damage presence identification of cable-supported bridges (Zhou *et al*. 2011a, Ni *et al.* 2015). As shown in Fig. 4, an ANN is configured as a multi-layer perceptron with 'bottleneck' hidden layer(s), and is trained to reproduce at the output layer, the patterns which are presented at the input layer. Thus the output layer must have the same number of the input nodes. As the hidden layers of the network have fewer nodes than the input and output layers, the ANN is forced to learn just the significant prevailing features of the input patterns (Rumelhart *et al.* 1986, Hinton 1989). When it is designated for structural damage detection, a series of measurement data of the healthy structure under normal environmental variations, $\boldsymbol{X} = \{X_1 X_2 \ldots\ldots X_n\}^T$, are required to train the network. In the case of using modal frequencies as input vector, each entry $X_i$ ($i$ = 1, 2, …,$n$) in $\boldsymbol{X}$ denotes a series of measured modal frequencies for the $i$th mode from the healthy structure under varying operational and environmental conditions. The ANN can be trained by using $\boldsymbol{X}$ as both input and output (Zhou *et al.* 2011a) or designating output samples that are different from $\boldsymbol{X}$ but yet derived from $\boldsymbol{X}$ (Ni *et al.* 2015). In the latter case, the output samples $\boldsymbol{Y} = \{Y_1 Y_2 \ldots\ldots Y_n\}^T$ can be obtained by (Ni *et al.* 2015)

$$Y_i = (X_i - m_i)\alpha + m_i \qquad (i = 1, 2, \cdots\cdots, n) \tag{1}$$

where $m_i$ is the mean of the $i$th entry $X_i$ of $\boldsymbol{X}$ over the input samples; the penalty factor $\alpha$, which is a tradeoff between amplifying the uncertainty effect and enhancing the significant features, is suggested to be 2 to 5. After training the ANN using $\boldsymbol{X}$ and $\boldsymbol{Y}$, the input samples $\boldsymbol{X}$ are fed again into the trained ANN to yield an output sequence $\hat{\boldsymbol{Y}}$, and the novelty index sequence for the training phase is obtained in terms of the Euclidean distance as

$$\lambda(\boldsymbol{Y}) = \left\| \boldsymbol{Y} - \hat{\boldsymbol{Y}} \right\| \tag{2}$$

When a new series of measurement data from an unknown state of the structure (damaged or

undamaged), $\boldsymbol{X}_t = \{X_{1t} X_{2t} \ldots\ldots X_{nt}\}^T$, are obtained, they are passed into the above trained ANN to yield an output sequence $\hat{\boldsymbol{Y}}_t$. The corresponding novelty index sequence for the testing phase is obtained by

$$\lambda(\boldsymbol{Y}_t) = \left\| \boldsymbol{Y}_t - \hat{\boldsymbol{Y}}_t \right\| \tag{3}$$

where $\boldsymbol{Y}_t = \{Y_{1t} Y_{2t} \ldots\ldots Y_{nt}\}^T$ is a vector having its $i$th entry as

$$Y_{it} = (X_{it} - m_i)\alpha + m_i \qquad (i = 1, 2, \cdots\cdots, n) \tag{4}$$

If the novelty index sequence in the testing phase deviates from that in the training phase, the occurrence of structural damage is alarmed; if they are indistinguishable, no damage is signaled.

### *3.2 ANN-based damage identification using combined modal parameters*

By using modal frequencies as input to ANNs, a simulation study on damage presence identification of the TMB has been conducted by assuming a total of 15 damage cases (Ni *et al.* 2015). The first three cases simulate the damage at the lateral and horizontal bearings between a bridge tower and the deck; the fourth and fifth are the damage at a side span cable and at an anchorage (shift of the anchorage), respectively; the sixth to eighth simulate the damage at a tower saddle (slippage of the saddle) and at a tower cross-beam (top cross-beam of the tower); the ninth to tenth are the damage at hangers (two mid-span hangers on the north and south sides, respectively); the eleventh to fourteenth simulate the damage at deck members; and the fifteenth simulates the damage at rail way beams. After merging modal categories (iv) and (v) into one group and merging modal categories (vi) and (vii) into one group, five ANNs were formulated where noisy/uncertain 'measured' data of modal frequencies for the intact structure and the structure in each damage case were generated by adding the computed modal frequencies from the FEM(without or with assumed damage) with normally distributed random noises with zero mean and 0.005 variance (about ±1.5% maximum error).

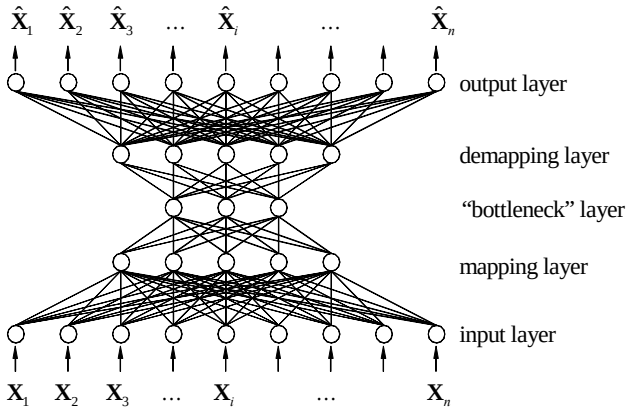


Fig. 4 Auto-associative neural network (ANN)

The simulation study showed that the ANNs by using modal frequencies as input vector were able to signal damage occurrence only when the maximum modal frequency change ratios caused by damage exceeded a certain value. Under the noise/uncertainty level of 0.005 variance, the damage is detectable only when the damage-caused maximum frequency change ratio for the concerned modes is larger than 0.3% (Ni *et al.* 2015). The damage at deck members could be identified only when severe damage occurred, i.e., Case 14 where two top chords, two bottom chords and two diagonal members were damaged simultaneously. The damage in Cases 11, 12 and 13 was undetectable by the above formulated ANNs. Actually, the damage-caused maximum frequency change ratios in Cases 11 to 14 are 0.1688%, 0.2030%, 0.0693% and 0.8843%, respectively.

In recognizing that the damage identification capability of the ANNs formulated using only modal frequencies is limited by the maximum modal frequency change ratio, we in the present study endeavor to re-formulate the ANNs by substituting combined modal parameters for modal frequencies as input vector. Without using a structural model, various combined modal parameters can be constructed by synthesizing measured modal frequencies and mode shape components (Ni *et al.* 2002, Ni *et al.* 2006). In the present study, modal flexibility coefficients substituting for modal frequencies are adopted as input vector to train ANNs due to the following reasons: (i) modal flexibility combines the information from both modal frequencies and mode shape components; and (ii) modal flexibility can be accurately estimated by using only the measured modal frequencies and incomplete mode shape components from a few low-order modes, because the modal contribution to flexibility decreases as frequency increases. With a limited number of measured modes and a few mode shape components, the flexibility matrix can be estimated by (Pandey and Biswas 1994, Toksoy and Aktan 1994)

$$[\boldsymbol{F}]_{p\times p} \approx [\boldsymbol{\Phi}]^T_{p\times m}[\boldsymbol{\Lambda}]_{m\times m}[\boldsymbol{\Phi}]_{m\times p} \tag{5}$$

where $m$ denotes the number of measured modes; and $p$ denotes the number of measured incomplete mode shape components (measured DOFs). $[\boldsymbol{\Lambda}]_{m\times m}$ is the measured modal eigenvalue matrix; and $[\boldsymbol{\Phi}]_{m\times p}$ is the measured mode shape matrix after mass-normalization.

In the present study, only the diagonal components of the measurement-derived flexibility matrix are used instead of modal frequencies as input feature to train ANN. That is

$$\boldsymbol{X} = Diag([\boldsymbol{F}]_{p\times p}) = \{F_{11} \cdots F_{ii} \cdots F_{pp}\}^T \tag{6}$$

and

$$F_{ii} = \sum_{k=1}^{m} \frac{\phi_{ik}^2}{\omega_k^2} \tag{7}$$

where $\omega_k$ ($k$ = 1, 2, ⋯, $m$) is the measured circular frequency of the $k$th mode; and $\phi_{ik}$ ($i$ = 1, 2, ⋯, $p$; $k$ = 1, 2, ⋯, $m$) is the measured mode shape component (after mass-normalization) of the $k$th mode at the $i$th location (DOF).

In the present study, it is assumed that merely the modal frequencies of the first five modes and the corresponding mode shape components at 15 DOFs located at the deck of the TMB are measured. As a result, only the flexibility coefficients at these 15 nodes are available. So the dimension of the input vector $\boldsymbol{X}$ to train ANNs is 15. The ‘measured’ flexibility coefficients of

the intact structure at the 15 DOFs are generated by adding the computed flexibility coefficients from the FEM and Eq. (7) with normally distributed random noises with zero mean and 0.005 variance. They are used as the input training samples $\boldsymbol{X}$ and to calculate the output training samples $\boldsymbol{Y}$ according to Eq. (1). Rather than formulating five ANNs as in the previous study, only one ANN is herein constructed with a node structure of 15-11-11-15 for damage occurrence detection. After training the ANN using the input samples $\boldsymbol{X}$ and the output samples $\boldsymbol{Y}$, the input samples $\boldsymbol{X}$ are passed again into the trained ANN to form a novelty index sequence in the training phase.

The input samples $\boldsymbol{X}_t$ for each damage case are generated in a similar way. By computing the modal frequencies and mode shape components of the first five modes from the FEM where the damage is incurred, the 'measured' flexibility coefficients of the damaged structure at the 15 DOFs are obtained by corrupting the analytical flexibility coefficients with normally distributed random noises with zero mean and 0.005 variance. They are fed into the trained ANN to obtain $\hat{\boldsymbol{Y}}_t$, from which the corresponding novelty index sequence for the testing phase is derived in accordance with Eq. (3) ($\boldsymbol{Y}_t$ wherein is obtained by Eq. (4)). A deviation of the novelty index sequence from the training to testing phases alarms the occurrence of damage. Only the detection results of Case 11 (damage at deck members) are presented here. The damage in Case 11 is simulated by loss of the stiffness of two longitudinal bottom chords near the mid-span of the TMB. For comparison, the novelty index sequences in both training and testing phases are first obtained by the five ANNs previously formulated with their input vector being modal frequencies (the modal assurance criterion was utilized to identify the correlated modes of the intact structure and the structure with assumed damage). As shown in Fig. 5, from all the five ANNs formulated using modal frequencies, the occurrence of damage in Case 11 cannot be flagged as the novelty index sequences between the training and testing phases are indistinguishable. Actually, the absolute maximum frequency change ratio caused by the damage in Case 11 is only 0.1688%.

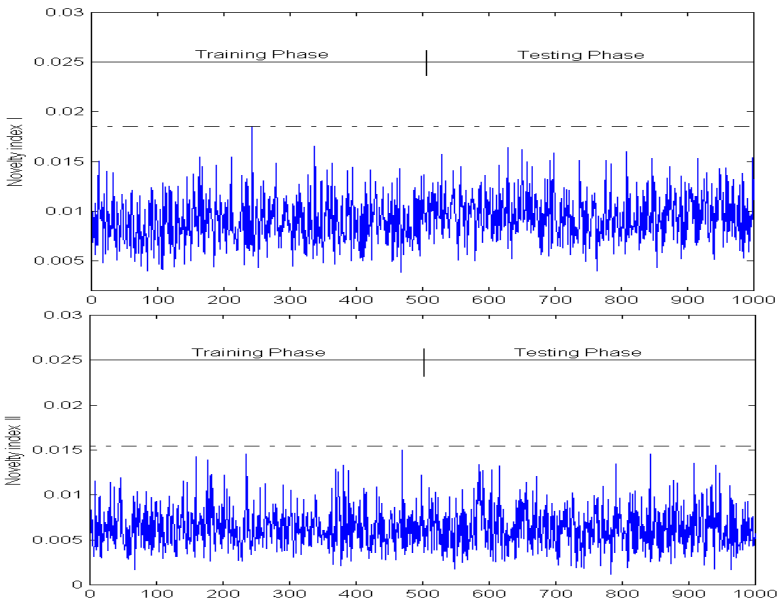


Continued-

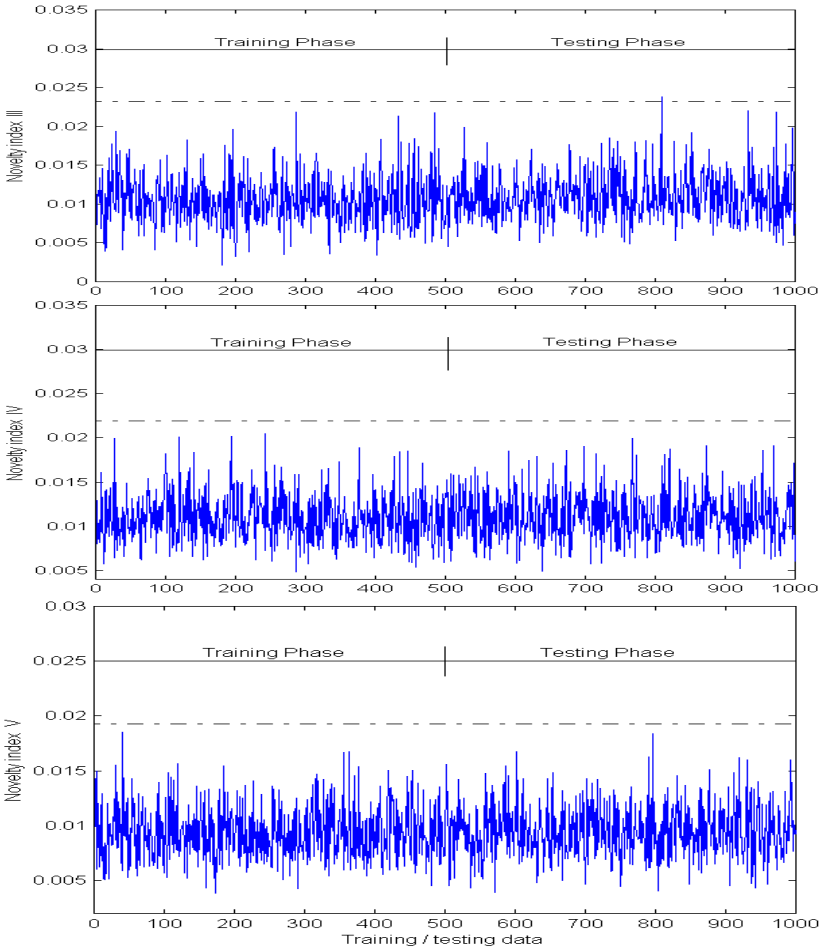


Fig. 5 Novelty index sequences formulated in terms of modal frequencies

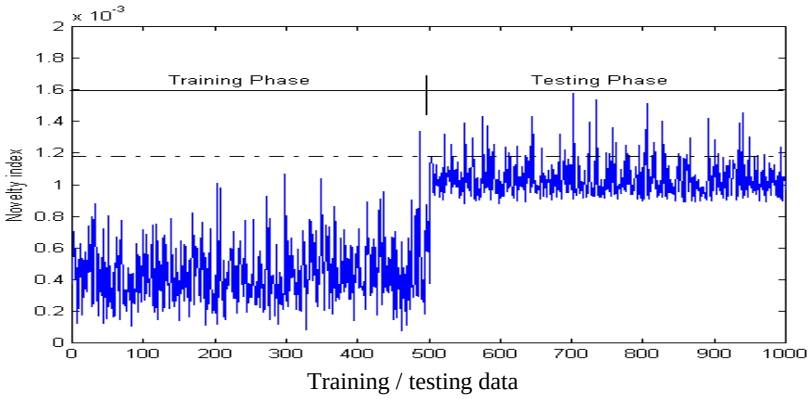


Fig. 6 Novelty index sequences formulated in terms of combined modal parameters

Fig. 6 shows the novelty index sequences in both training and testing phases for the same case obtained by the ANN formulated with its input vector being flexibility coefficients. It is observed that the ANN formulated using flexibility coefficients can unambiguously signal the occurrence of damage in Case 11, evidenced by that the novelty index sequence in the testing phase deviates unambiguously from the sequence in the training phase. This means that when the flexibility coefficients derived using measured modal frequencies and incomplete mode shape components are used as input vector, the formulated ANN is able to alarm damage incurred at deck members even when the damage-induced maximum frequency change ratio is less than 0.3%. It is therefore concluded that the ANN formulated using flexibility coefficients provides a better capability than that formulated using modal frequencies in identifying the occurrence of minor structural damage in operation with noisy measurement data.

## 4. Damage localization by PNNs with different design of smoonthing parameter

### *4.1 Formulation*

The PNN (Specht 1990, Specht 1996) performs the Bayesian decision analysis with the Parzen windows estimator cast into an artificial neural network framework. When applied to damage identification, the PNN uses exemplars from the undamaged and damaged system to establish whether a new measurement of unknown origin comes from the undamaged class or the damaged class. Because the PNN approach describes measurement data in a Bayesian probabilistic approach, it shows great promise for structural damage detection in noisy conditions. For a multi-category classification problem with a number of categories $\theta_1$, $\theta_2$, $\cdots\theta_q$, $\cdots\theta_s$, the Bayesian decision rule to decide the state of nature $\theta \in \theta_q$ based on a set of measurements represented by a $p$-dimensional vector $\boldsymbol{X} = \{x_1 x_2 \cdots x_i \cdots x_p\}^T$ can be described as (Webb and Copsey 2011)

$$d(\boldsymbol{X}) \in \theta_q \quad \text{if} \quad h_q l_q f_q(\boldsymbol{X}) > h_k l_k f_k(\boldsymbol{X}) \quad \text{for all} \quad k \neq q \tag{8}$$

where $d(\boldsymbol{X})$ is decision on the test vector $\boldsymbol{X}$; $h_q$ and $h_k$ are prior probabilities of categories $\theta_q$ and $\theta_k$, respectively; $l_q$ is the loss associated with misclassifying $d(\boldsymbol{X}) \notin \theta_q$ when $\theta \in \theta_q$ and $l_k$ is the loss associated with misclassifying $d(\boldsymbol{X}) \notin \theta_k$ when $\theta \in \theta_k$; $f_q(\boldsymbol{X})$ and $f_k(\boldsymbol{X})$ are the probability density functions (PDFs) for categories $\theta_q$ and $\theta_k$, respectively. For damage detection problem, $h$ and $l$ are usually assumed to be equal for all categories. Therefore, the key to using Eq. (8) is the ability to estimate PDFs based on training patterns. The method of Parzen windows can be used to estimate the PDFs in terms of kernel density estimators (Wasserman 1993)

$$f_q(\boldsymbol{X}) = \frac{1}{n_q (2\pi)^{p/2} \sigma^p} \sum_{i=1}^{n_q} \exp\left[ -\frac{(\boldsymbol{X} - \boldsymbol{X}_{qi})^T (\boldsymbol{X} - \boldsymbol{X}_{qi})}{2\sigma^2} \right] \tag{9}$$

where $\boldsymbol{X}$ is the test vector to be classified; $f_q(\boldsymbol{X})$ the value of the PDF of category $q$ at point $\boldsymbol{X}$; $n_q$ the number of training vectors in category $q$; $p$ the dimensionality of the training vectors; $\boldsymbol{X}_{qi}$ the $i$th training vector from category $q$; and $\sigma$ the smoothing parameter.

Fig. 7 illustrates the architecture of a PNN that consists of three layers. An input vector $\boldsymbol{X} = \{x_1 x_2 \cdots x_i \cdots x_p\}^T$ to be classified is applied to the neurons of the distribution (input) layer that just supply the input values to all the pattern units. In the pattern layer, each neuron forms a dot

product of the pattern vector $\boldsymbol{X}$ with a weight vector $\boldsymbol{W}_j$ of a given class, $z_j = \boldsymbol{X}\cdot\boldsymbol{W}_j$, and then performs a nonlinear operation on $z_j$ before output to the summation layer. The activation function used here is $g(z_j) = \exp[(z_j-1)/\sigma^2]$. Each neuron in the summation layer receives all pattern layer outputs associated with a given class. For instance, the output of the summation layer neuron corresponding to class $q$ is

$$f_q(\boldsymbol{X}) = \sum_{j=1}^{n_q} z_{qj} = \sum_{j=1}^{n_q} \exp[(\boldsymbol{X}\cdot\boldsymbol{W}_{qj} - 1)/\sigma^2] \tag{10}$$

It can be proven that if the weight vector $\boldsymbol{W}_{qj}$ is taken as the training vector $\boldsymbol{X}_{qj}$ corresponding to the class $q$ and both $\boldsymbol{X}$ and $\boldsymbol{X}_{qj}$ are normalized with $\boldsymbol{X}\cdot\boldsymbol{X} = \boldsymbol{X}_{qj}\cdot\boldsymbol{X}_{qj} = 1$, then the resulting output in the summation layer neuron, Eq. (10), is the same form as Eq. (9). That is, the kernel density estimators for PDFs have been cast into the PNN by setting the weight vectors as the corresponding training vectors. Since the PNN directly casts the PDFs of training samples in the network, it is convenient for dealing with noisy measurement data when applied for damage identification. A salient feature of the PNN is that it can explicitly accommodate the noise/uncertainty characteristic as neuro-weights in the configured network.

### *4.2 PNN-based damage identification using adaptive smoothing parameter*

The PNN has been proposed by the authors for damage localization of cable-supported bridges by using a constant smoothing parameter $\sigma$ in Eq. (10) for all pattern classes and input variables (Zhou *et al.* 2014). It was found that when the noise/uncertainty level exceeded a certain value, the identification accuracy by the PPN was significantly dropped. Actually, the smoothing parameter $\sigma$ in Eqs. (9) and (10) represents the standard deviation of the Gaussian kernels in the Parzen window estimator. A small $\sigma$ causes the estimated density function to exhibit sharply peaks whereas a large $\sigma$ provides greater smoothing between points in the density estimation. As a result, the choice of $\sigma$-parameter would have an influence on the performance of PNN. In the present study, effort is made to enhance the damage identification capability of the PNN through optimally determining different values of the smoothing parameter for different pattern classes. For this purpose, Eq. (9) is re-defined by introducing the weighed Euclidean distance separating the test vector $\boldsymbol{X}$ from the training vector $\boldsymbol{X}_{qi}$ for category $q$ as follows

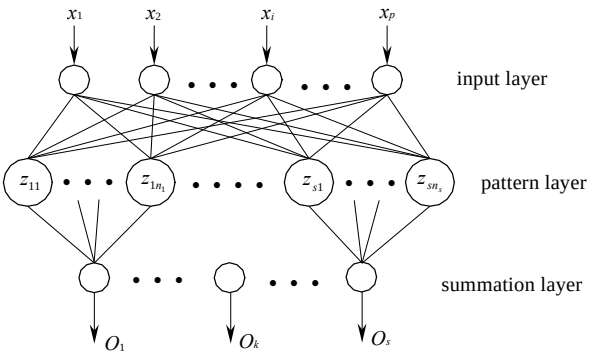


Fig. 7 Probabilistic neural network (PNN)

$$D(\boldsymbol{X}, \boldsymbol{X}_{qi}) = \sum_{j=1}^{p} \left( \frac{\boldsymbol{X}(j) - \boldsymbol{X}_{qi}(j)}{\sigma_j} \right)^2 \tag{11}$$

and the density estimator with the Gaussian kernel function is obtained as

$$f_q(\boldsymbol{X}) = \frac{1}{n_q} \sum_{i=1}^{n_q} \exp(-D(\boldsymbol{X}, \boldsymbol{X}_{qi})) \tag{12}$$

Given the training vectors and a set of the smoothing parameters for the variables, we can compute density estimates from Eq. (12) for each class at the test vector point. In order to determine the optimal smoothing parameters, a continuous error criterion that allows computing the derivatives with respect to the smoothing parameters has been established as (Masters 1995)

$$e_q(\boldsymbol{X}) = [1 - b_q(\boldsymbol{X})]^2 + \sum_{j \neq q} [b_j(\boldsymbol{X})]^2 \tag{13}$$

where the Bayesian confidence $b_q(\boldsymbol{X})$ is obtained by

$$b_q(\boldsymbol{X}) = \frac{h_q(\boldsymbol{X})}{v(\boldsymbol{X})} \tag{14}$$

$$v(\boldsymbol{X}) = \sum_{q=1}^{s} h_q(\boldsymbol{X}) \tag{15}$$

$$h_q(\boldsymbol{X}) = \sum_{i=1}^{n_q} \delta_q(i) \exp(-D(\boldsymbol{X}, \boldsymbol{X}_{qi})) \tag{16}$$

$$\delta_q(i) = \begin{cases} 1 & \textit{if training vector i is a member of class q} \\ 0 & \textit{otherwise} \end{cases} \tag{17}$$

Thus the optimal smoothing parameters can be searched by an optimization method such as the gradient descent technique and the genetic algorithm (GA).

A simulation study of applying the PNN to locate damage incurred at the deck members of the TMB is then conducted. To facilitate the damage localization, the main span deck is divided into 16 segments (each including 4 or 5 deck units) as listed in Table 1. The damage to the deck members within a same segment is classified as one pattern class. As a result, there are totally 16 pattern classes, i.e., $s$ = 16. In recognizing that the modal frequencies can be easily and accurately measured, each pattern class is characterized by the modal frequency change ratios between the undamaged and damaged states. That is, the modal frequency change ratios are used as the entries of the input vector $\boldsymbol{X} = \{x_1\, x_2 \cdots x_i \cdots x_p\}^T$. For the purpose of comparison, the input vector was initially designed to comprise the first 10 and 20 modal frequencies respectively. Later the modal frequencies of the 6th, 8th, 16th, 17th and 20th were withdrawn from the input vectors because their change ratios were almost zero. Finally, the number of input vectors is 8 and 15 respectively, i.e., $p$ = 8 and 15.

In order to obtain the training vectors, for each pattern class two damage scenarios with the damage within the same segment but different units (refer to Table 1) are introduced in the FEM and the corresponding modal frequency change ratios are evaluated. Each set of the computed modal parameters are then added with a random sequence to form the training vectors

$$x_i = x_i^a \times (1 + \varepsilon R) \tag{18}$$

where $x_i$ is a component of the noise polluted training vectors; $x_i^a$ is the analytically computed modal frequency change ratio for a certain pattern class; $R$ is a normally distributed random variable with zero mean and unity variance; $\varepsilon$ is an index representing the noise level.

50 sets of modal frequency change ratios are randomly produced for each damage scenario. There are therefore 50×2=100 sets of training vectors for each pattern class, i.e., $n_1 = n_2 = \cdots = n_{16} = 100$. After entering the noise-polluted training vectors of all pattern classes to the distribution (input) layer, the PNN for damage localization is trained. When presenting on the network a new input vector (test vector) consisting of measured modal frequency ratios of unknown source, the configured PNN outputs in the summation layer the PDF estimate for each pattern class at the test vector point. The pattern class with the largest PDF implies the class of the current input (test) vector and indicates the damage location.

The test vectors for the damage localization simulation study are produced in a similar way. A total of 16 damage scenarios, with one for each deck segment (pattern class), are examined. As shown in Table 1, the testing damage scenario for each pattern class is incurred at the deck unit different from the corresponding training damage scenarios. The analytical modal frequency ratios when incurring damage at each deck segment in turn are calculated and then polluted with random noise to obtain the 'measured' test vectors. The random noise sequences used to contaminate the training samples and the testing samples are independent but with identical level. For each testing damage scenario, 200 sets of noise-corrupted test vectors are generated. Therefore, a total of 200×16=3,200 test vectors are used in the damage localization study.

For comparison, the damage identification results are obtained by using a constant smoothing parameter and using different optimized smoothing parameters for different pattern classes and input variables. A previous study by Specht (1990) indicated that a satisfactory pattern classification could be achieved by the PNN when taking the value of the smoothing parameter between 0.2 and 0.3, and therefore the smoothing parameter in the constant parameter case is taken as 0.25 in this study. The optimal smoothing parameters for different pattern classes in the adaptive parameter case are determined by the GA.

Table 1 Training and Testing Samples for PNN

| Pattern class No. | | 1 | 2 | 3 | 4 | 5 | 6 | 7 | 8 | 9 | 10 | 11 | 12 | 13 | 14 | 15 | 16 |
|---|---|---|---|---|---|---|---|---|---|---|---|---|---|---|---|---|---|
| Deck units involved | | 1-4 | 5-9 | 10-14 | 15-19 | 20-24 | 25-29 | 30-34 | 35-38 | 39-42 | 43-47 | 48-52 | 53-57 | 58-62 | 63-67 | 68-72 | 73-76 |
| Training samples | Location | 2,4 | 7,8 | 10,12 | 15,17 | 20,22 | 25,27 | 30,32 | 36,38 | 39,41 | 43,45 | 48,50 | 53,55 | 58,60 | 63,65 | 68,70 | 73,75 |
| | Data length | 50×2 | 50×2 | 50×2 | 50×2 | 50×2 | 50×2 | 50×2 | 50×2 | 50×2 | 50×2 | 50×2 | 50×2 | 50×2 | 50×2 | 50×2 | 50×2 |
| Testing samples | Location | 3 | 6 | 11 | 16 | 21 | 26 | 31 | 37 | 40 | 44 | 49 | 54 | 59 | 64 | 69 | 74 |
| | Data length | 200 | 200 | 200 | 200 | 200 | 200 | 200 | 200 | 200 | 200 | 200 | 200 | 200 | 200 | 200 | 200 |

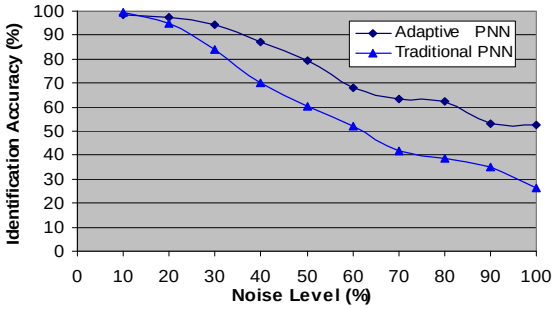


Fig. 8 Identification accuracy (IA) versus noise level ($\varepsilon$)

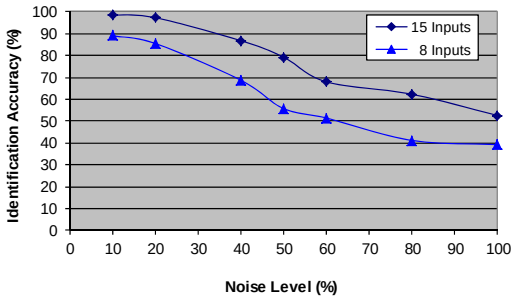


Fig. 9 Identification accuracy (IA) under different input vectors

Table 2 Number of Times with Correct Identification and IA Ratio

| Pattern class No. | 1 | 2 | 3 | 4 | 5 | 6 | 7 | 8 | 9 | 10 | 11 | 12 | 13 | 14 | 15 | 16 | IA ratio |
|---|---|---|---|---|---|---|---|---|---|---|---|---|---|---|---|---|---|
| Testing sample No. | 200 | 200 | 200 | 200 | 200 | 200 | 200 | 200 | 200 | 200 | 200 | 200 | 200 | 200 | 200 | 200 | (%) |
| $\varepsilon$=100% | 115 (23) | 129 (193) | 118 (27) | 96 (49) | 96 (68) | 72 (0) | 75 (6) | 187 (106) | 105 (42) | 89 (65) | 84 (86) | 72 (7) | 109 (31) | 106 (69) | 157 (38) | 75 (31) | 52.66 (26.28) |
| $\varepsilon$=90% | 126 (38) | 123 (121) | 83 (25) | 84 (50) | 97 (75) | 89 (36) | 97 (45) | 186 (143) | 116 (85) | 92 (36) | 89 (81) | 74 (36) | 85 (54) | 101 (99) | 167 (134) | 95 (56) | 53.25 (34.81) |
| $\varepsilon$=80% | 140 (55) | 151 (161) | 119 (70) | 109 (62) | 104 (91) | 122 (100) | 136 (68) | 194 (156) | 129 (81) | 109 (55) | 109 (55) | 94 (0) | 97 (55) | 114 (84) | 158 (130) | 114 (21) | 62.34 (38.88) |
| $\varepsilon$=70% | 153 (31) | 132 (189) | 142 (104) | 103 (62) | 101 (31) | 90 (28) | 142 (49) | 197 (157) | 136 (95) | 128 (63) | 112 (113) | 99 (118) | 102 (92) | 99 (57) | 166 (88) | 127 (60) | 63.41 (41.78) |
| $\varepsilon$=60% | 157 (50) | 142 (200) | 124 (89) | 117 (97) | 112 (98) | 142 (75) | 159 (105) | 200 (174) | 138 (126) | 135 (60) | 135 (103) | 118 (110) | 116 (89) | 115 (135) | 161 (79) | 106 (80) | 68.03 (52.19) |
| $\varepsilon$=50% | 171 (92) | 186 (183) | 169 (118) | 148 (115) | 142 (86) | 135 (67) | 170 (79) | 200 (192) | 157 (119) | 171 (123) | 139 (133) | 124 (146) | 141 (113) | 162 (128) | 169 (129) | 154 (110) | 79.31 (60.41) |
| $\varepsilon$=40% | 183 (123) | 199 (188) | 184 (146) | 170 (133) | 173 (107) | 160 (95) | 180 (147) | 200 (200) | 171 (148) | 186 (123) | 152 (160) | 149 (134) | 153 (123) | 181 (166) | 185 (137) | 152 (111) | 86.88 (70.03) |
| $\varepsilon$=30% | 195 (164) | 195 (199) | 199 (181) | 198 (164) | 198 (139) | 175 (143) | 198 (183) | 200 (200) | 194 (169) | 195 (170) | 174 (180) | 183 (186) | 188 (180) | 185 (193) | 190 (137) | 154 (111) | 94.41 (83.97) |
| $\varepsilon$=20% | 200 (186) | 196 (200) | 200 (199) | 199 (198) | 196 (192) | 187 (179) | 200 (197) | 200 (200) | 200 (196) | 200 (189) | 185 (198) | 163 (198) | 198 (192) | 200 (198) | 195 (142) | 198 (173) | 97.38 (94.91) |
| $\varepsilon$=10% | 200 (200) | 198 (200) | 200 (200) | 200 (200) | 200 (200) | 162 (200) | 200 (200) | 200 (200) | 200 (200) | 200 (200) | 200 (200) | 198 (200) | 200 (200) | 200 (200) | 200 (181) | 200 (197) | 98.69 (99.31) |

Because the PNN describes the data in a probabilistic approach, the identification accuracy should be evaluated in a statistical manner. Table 2 provides the number of times with correct identification and the identification accuracy (IA) ratios for the total 3,200 testing samples by the PNN with adaptive smoothing parameters, and the results obtained by the PNN with a constant smoothing parameter are also provided in the parentheses for comparison. The 15 modal frequency change ratios are used as input vector to obtain the results. Here the IA ratio is defined as the ratio of the total number of times with correct identification for all testing damage scenarios to the total number of the testing samples (3,200). Fig. 8 shows the identification accuracy (IA) versus noise level ($\varepsilon$). From Table 2 and Fig. 8 it is found that when the noise/uncertainty level is low ($\varepsilon$=10%), the PNN with adaptive smoothing parameters (adaptive PNN) performs similarly as the PNN with a constant smoothing parameter (traditional PNN) in regard to the identification accuracy, both giving damage identification results with a high fidelity. With the increase of the noise/uncertainty level, however, the adaptive PNN greatly outperforms the traditional PNN in terms of the identification accuracy. In particular, the adaptive PNN performs much better than the traditional PNN in the case of high noise level. It is very encouraging to note that the difference of the IA ratios between the adaptive PNN and the traditional PNN increases with the increase of the noise/uncertainty level.

Fig. 9 shows the IA ratios of the adaptive PNN when using 8 and 15 modal frequency change ratios as input vector, respectively. It is seen that the identification accuracy using the 15 modal frequencies is obviously better than that using the 8 modal frequencies. It is also observed that this improvement of the identification accuracy when using more modal frequencies is almost irrelative to noise level. Under heavy noise conditions, therefore, it is preferable to use a relatively large number of modal frequencies as input vector to achieve the identification with confidence.

## 5. Conclusions

In this study, efforts were made to refine the damage identification capability of the auto-associative neural network (ANN) technique and the probabilistic neural network (PNN) technique in application to a suspension bridge. The ANN technique is promising for real applications because it eschews structural model and the measured modal frequencies are sufficient for damage alarming. When applied to long-span cable-supported bridges, however, the ANNs formulated using modal frequencies might fail to alarm minor damage if the damage-induced modal frequency change ratio is very low. This study formulated combined modal parameters in terms of the measured modal frequencies and incomplete mode shape components from a few low-order modes, and adopted the combined modal parameters to train ANNs for damage occurrence identification. The simulation results of the suspension TMB indicate that the ANNs formulated using the combined modal parameters perform better than the ANNs formulated using modal frequencies in detecting the occurrence of minor structural damage in operation with noisy measurement data.

The PNN technique for damage localization requires a structural model. Different from the ANN, the PNN explicitly accommodates the noise/uncertainty characteristic as neuro-weights in the configured network. As it implements a Bayesian classification by combining the Bayesian decision rule with the Parzen window estimator, the selection of the smoothing parameter is essential for damage classification. It has been shown that when applied to cable-supported bridges, the damage identification capability of the PNN with a constant smoothing parameter might be

sharply deteriorated with increasing noise/uncertainty level. This study introduced an adaptive strategy to determine different optimized smoothing parameters for different pattern classes, with the purpose of improving the damage localization (classification) capability. The numerical simulation results of the suspension TMB show that the identification accuracy of the adaptive PNN is greatly better than the traditional PNN when the measurement data are heavily polluted. The identification accuracy is enhanced when more modal frequencies are used as input vector to the PNN. The improvement of the identification accuracy when using more modal frequencies is almost irrelative to the noise/uncertainty level.

## Acknowledgments

The work described in this paper was supported by a grant from the Research Grants Council of the Hong Kong Special Administrative Region, China (Project No. PolyU 5224/13E).

## References

Aktan, A.E., Chase, S., Inman, D. and Pines, D.D. (2001), *Monitoring and managing the health of infrastructure systems*, Health Monitoring and Management of Civil Infrastructure Systems, (Eds., S.B. Chase and A.E. Aktan), Proceedings of SPIE Vol. 4337, SPIE, Bellingham, Washington, USA (CD-ROM).

Beard, A.S. (1995), "Tsing Ma Bridge, Hong Kong", *Struct. Eng. Int.*, **5**, 138-140.

Beard, A.S. and Young, J.S. (1995), "Aspects of the design of the Tsing Ma Bridge", *Bridges into the 21st Century: Proceedings of the International Conference*, The Hong Kong Institution of Engineers, Hong Kong.

Brownjohn, J.M.W. (2007), "Structural health monitoring of civil infrastructure", *Philos. T. R. Soc. A*, **365**, 589-622.

Catbas, F.N. (2009), *Structural health monitoring: applications and data analysis*, Structural Health Monitoring of Civil Infrastructure Systems, (Eds., V.M. Karbhari and F. Ansari), Woodhead Publishing, Cambridge, UK.

DeWolf, J.T., Lauzon, R.G. and Culmo, M.P. (2002), "Monitoring bridge performance", *Struct. Health Monit.*, **1**, 129-138.

Fujino, Y., Siringoringo, D.M. and Abe, M. (2009), "The needs for advanced sensor technologies in risk assessment of civil infrastructures", *Smart Struct. Syst.*, **5**(2), 173-191.

Glisic, B., Inaudi, D. and Casanova, N. (2009), "SHM process – lessons learned in 250 SHM projects", *Proceedings of the 4th International Conference on Structural Health Monitoring and Intelligent Infrastructure*, Zurich, Switzerland (CD-ROM).

Hinton, G.E. (1989), "Connectionist learning procedures", *Artif. Intell.*, **40**(1-3), 185-234.

Kim, J.T., Huynh, T.C., and Lee, S.Y. (2014), "Wireless structural health monitoring of stay cables under two consecutive typhoons", *Struct. Monit. Maint.*, **1**(1), 47-67.

Ko, J.M. and Ni, Y.Q. (2005), "Technology developments in structural health monitoring of large-scale bridges", *Eng. Struct.*, **27**(12), 1715-1725.

Ko, J.M., Sun, Z.G. and Ni, Y.Q. (2002), "Multi-stage identification scheme for detecting damage in cable-stayed Kap Shui Mun Bridge", *Eng. Struct.*, **24**(7), 857-868.

Li, H.N., Yi, T.H., Ren, L., Li, D.S., and Huo, L.S. (2014), "Reviews on innovations and applications structural health monitoring for infrastructures", *Struct. Monit. Maint.*, **1**(1), 1-45.

Masters, T. (1995), *Advanced Algorithms for Neural Networks: A C++ Sourcebook*, John Wiley & Sons, Chichester, UK.

Minardo, A., Coscetta, A., Porcaro, G., Giannetta, D., Bernini, R. and Zeni, L. (2014), "Distributed optical

fiber sensors for integrated monitoring of railway infrastructures", *Struct. Monit. Maint.*, **1**(2), 173-182.
Ni, Y.Q., Wang, B.S. and Ko, J.M. (2002), "Constructing input vectors to neural networks for structural damage identification", *Smart Mater. Struct.*, **11**(6), 825-833.
Ni, Y.Q., Wang, J. and Chan, T.H.T. (2015), "Structural damage alarming and localization of cable-supported bridges using multi-novelty indices: a feasibility study", *Struct. Eng. Mech.*, **54**(2), in press.
Ni, Y.Q., Wong, K.Y. and Xia, Y. (2011), "Health checks through landmark bridges to sky-high structures", *Adv. Struct. Eng.*, **14**(1), 103-119.
Ni, Y.Q., Xia, Y., Liao, W.Y. and Ko, J.M. (2009), "Technology innovation in developing the structural health monitoring system for Guangzhou New TV Tower", *Struct. Control Health Monit.*, **16**(1), 73-98.
Ni, Y.Q., Zhou, H.F., Chan, K.C. and Ko, J.M. (2008), "Modal flexibility analysis of cable-stayed Ting Kau Bridge for damage identification", *Comput. - Aided Civ. Inf.*, **23**(3), 223-236.
Ni, Y.Q., Zhou, X.T. and Ko, J.M. (2006), "Experimental investigation of seismic damage identification using PCA-compressed frequency response functions and neural networks", *J. Sound Vib.*, **290**(1-2), 242-263.
Oh, C.K., Sohn, H. and Bae, I.H. (2009), "Statistical novelty detection within the Yeongjong suspension bridge under environmental and operational variations", *Smart Mater. Struct.*, **18**(12), 125022 (9 pp).
Pandey, A.K. and Biswas, M. (1994), "Damage detection in structures using changes in flexibility", *J. Sound Vib.*, **169**(1), 3-17.
Rumelhart, D.E., Hinton, G.E. and Williams, R.J. (1986), *Learning internal representations by error propagation*, Parallel Distributed Processing: Explorations in the Microstructure of Cognition, (Eds., D.E. Rumelhart and J.L. McClelland), The MIT Press, Cambridge, Massachusetts, USA.
Specht, D.F. (1990), "Probabilistic neural networks", *Neural Networks*, **3**(1), 109-118.
Specht, D.F. (1996), *Probabilistic neural networks and general regression neural networks*, Fuzzy Logic and Neural Network Handbook, (Ed., C.H. Chen), McGraw-Hill, New York, USA.
Toksoy, T. and Aktan, A.E. (1994), "Bridge-condition assessment by modal flexibility", *Exp. Mech.*, **34**(3), 271-278.
Wang, M.L. and Yim, J. (2010), "Sensor enriched infrastructure system", *Smart Struct. Syst.*, **6**(3), 309-333.
Wasserman, P.D. (1993), *Advanced Methods in Neural Computing*, Van Nostrand Reinhold, New York, USA.
Webb, A.R. and Copsey, K.D. (2011), *Statistical Pattern Recognition*, 3rd Ed., John Wiley & Sons, Chichester, UK.
Wong, K.Y. (2004), "Instrumentation and health monitoring of cable-supported bridges", *Struct. Control Health Monit.*, **11**(2), 91-124.
Yan, A.M., De Boe, P. and Golinval, J.C. (2004), "Structural damage diagnosis by Kalman model based on stochastic subspace identification", *Struct. Health Monit.*, **3**(2), 103-119.
Yun, C.B., Lee, J.J. and Koo, K.Y. (2011), "Smart structure technologies for civil infrastructures in Korea: recent research and applications", *Struct. Infrastruct. E.*, **7**(9), 673-688.
Zhou, H.F., Ni, Y.Q. and Ko, J.M. (2011a), "Eliminating temperature effect in vibration-based structural damage detection", *J. Eng. Mech. - ASCE*, **137**(12), 785-796.
Zhou, H.F., Ni, Y.Q. and Ko, J.M. (2011b), "Structural damage alarming using auto-associative neural network technique: exploration of environment-tolerant capacity and setup of alarming threshold", *Mech. Syst. Signal Pr.*, **25**(5), 1508-1526.
Zhou, H.F., Ni, Y.Q. and Ko, J.M. (2013), "Structural health monitoring of the Jiangyin Bridge: system upgrade and data analysis", *Smart Struct. Syst.*, **11**(6), 637-662.
Zhou, X.T., Ni, Y.Q. and Zhang, F.L. (2014), "Damage localization of cable-supported bridges using modal frequency data and probabilistic neural network", *Math. Probl. Eng.*, Article ID 837963 (10pp).